DESTRUCTIVE EXAMINATION OF SHIPPING PACKAGE 9975-02101

W. L. Daugherty

May 2016

SRNL-STI-2016-00209, Revision 0

DISCLAIMER

Printed in the United States of America

Prepared for
U.S. Department of Energy

SRNL-STI-2016-00209
Revision 0

Keywords: *K-Area*
Surveillance
9975 Shipping Package

Retention: *Permanent*

DESTRUCTIVE EXAMINATION OF SHIPPING PACKAGE 9975-02101

W. L. Daugherty

May 2016

Prepared in conjunction with work accomplished under contract number DE-AC09-08SR22470 with the U.S. Department of Energy (DOE) Office of Environmental Management (EM).

Savannah River National Laboratory™
OPERATED BY SAVANNAH RIVER NUCLEAR SOLUTIONS

DESTRUCTIVE EXAMINATION OF SHIPPING PACKAGE 9975-02101

APPROVALS:

W. L. Daugherty _____ Date _____
Author, Materials Science and Technology

T. E. Skidmore _____ Date _____
Technical Review, Materials Science and Technology

K. A. Dunn _____ Date _____
Pu Surveillance Program Authority, Materials Science and Technology

G. T. Chandler _____ Date _____
Manager, Materials App & Process Tech

E. R. Hackney _____ Date _____
NMM Engineering

REVIEWS:

D. R. Leduc _____ Date _____
Savannah River Packaging Technology

J. W. McEvoy _____ Date _____
9975 Shipping Package Design Authority

Summary

Destructive and non-destructive examinations have been performed on the components of shipping package 9975-02101 as part of the comprehensive Model 9975 package surveillance program. This package is one of ten high-wattage packages that were selected for field surveillance in FY15, and was identified to contain several non-conforming conditions, including:

- Water stains on the upper fiberboard subassembly,
- A moldy smell, with mold located on the upper fiberboard subassembly,
- The axial gap exceeded the 1 inch maximum criterion, and
- A dimension calculated from fiberboard and shield heights failed the specified criterion.

Further examination and testing in SRNL confirmed these observations, and identified several additional conditions:

- Mold and excessive moisture around the bottom of the lower fiberboard subassembly,
- Corrosion along the bottom and lower side of the overpack drum (including penetration through a single wall thickness),
- Splitting and cracking of the bottom fiberboard layer due to handling and partial drying after unloading, and
- The inside diameter of the lead shield was larger than the specified range.

Most of these conditions (mold, stains, drum corrosion, calculated fiberboard dimensions and fiberboard damage) relate to the accumulation of water in the outer and lower portions of the cane fiberboard assembly. In the short term, this causes local but reversible changes in the fiberboard properties. Long-term effects can include the permanent loss of fiberboard properties (thus far observed only in the bottom fiberboard layers) and reduced drum integrity due to corrosion. The observed conditions must be fully evaluated by KAC to ensure the safety function of the package is being maintained. Three of the other nine FY15 high-wattage packages examined in the K-Area Complex showed similar behavior. Corrosion of the overpack drum has been seen primarily in those packages with relatively severe fiberboard degradation. Visual examination of the drums in storage for external corrosion should be considered as a screening tool to identify additional packages with potential fiberboard degradation. Where overpack drum corrosion has been observed, it is typically heaviest adjacent to the stitch welds along the bottom edge. It is possible that changes to the stitch weld design would reduce the degree of corrosion in this area, but would not eliminate it.

Several factors can contribute to the concentration of moisture in the fiberboard, including higher than average initial moisture content, higher internal temperature (due to internal heat load and placement with the array of packages), and the creation of additional moisture as the fiberboard begins to degrade.

Introduction

The Savannah River Site (SRS) stores packages containing plutonium (Pu) materials in the K-Area Complex (KAC). The Pu materials are packaged per the DOE 3013 Standard and stored within Model 9975 shipping packages in KAC.

The KAC facility DSA (Documented Safety Analysis) [1] credits the Model 9975 package to perform several safety functions, including criticality prevention, impact resistance, containment, and fire resistance to ensure the plutonium materials remain in a safe configuration during normal and accident conditions. The Model 9975 package is expected to perform its safety function for at least 15 years in the storage environment [2]. The DSA recognizes the degradation potential for the materials of package construction over time in the KAC storage environment and requires an assessment of materials performance to validate the assumptions of the analysis and ultimately predict service life.

As part of the comprehensive Model 9975 package surveillance program [3-4], destructive examination of package 9975-02101 was performed following field surveillance in accordance with Reference [5]. Field surveillance of the Model 9975 package in KAC included nondestructive examination of the drum, fiberboard, lead shield and containment vessels [6]. Results of the field surveillance are provided in Attachment 1.

Package History

Package 9975-02101 was loaded with plutonium oxide material packaged at RFETS in April 2003 in accordance with DOE-STD-3013 and received into KAC in June 2003. The contents generated approximately 14.5 watts heat load. Routine field surveillance was performed on August 17, 2015. After transfer to SRNL, the package was examined further on August 20, 2015. Results of this examination are documented in Reference 7. On January 26, 2016, 9975-02101 was identified as the package selected for destructive examination. DE activities were performed between February 1 and March 16, 2016.

Discussion

The results of the field surveillance [8] were reviewed. Four items were identified as unsatisfactory in the field surveillance:

- Water stains were observed on the upper fiberboard subassembly.
- A moldy smell was evident, with mold located on ¼ of the upper fiberboard subassembly outer circumference.
- The axial gap (1.659 inch) exceeded the 1 inch maximum criterion.
- The difference between the upper fiberboard subassembly inside height and the lower fiberboard subassembly height from lower step to top of lead shield (0.424 inch) was less than the specified minimum 0.425 inch.

As the package was first opened in SRNL and components removed, each component was marked to identify its orientation within the package. For components that were removed during the field surveillance, their orientation at the time of this examination probably bears no relation to their orientation while stored in KAC. However, the bottom fiberboard subassembly and lead shield would likely have remained in the same orientation they occupied in KAC.

Examination activities are documented through photographs, data sheets, and other documents. This documentation is maintained in a laboratory notebook [9]. The following examination activities were performed:

Fiberboard physical properties:

The weight and dimensions of the top and bottom fiberboard subassemblies were measured. The weight of the top subassembly was 11.906 kg (26.25 lb). During the field surveillance, the measured weight of the top subassembly was 26.3 lb. These two values are in good agreement. Weight and dimension data are recorded in Table 1.

The air shield was cut and peeled back at four locations to permit accurate measurement of the top fiberboard subassembly dimensions. In order to calculate the density of each subassembly, nominal dimensions were assumed for the aluminum bearing plates and air shield. The calculated densities (0.264 g/cc top subassembly, 0.291 g/cc bottom subassembly) meet the limit for the criticality control function, 0.20 g/cc minimum [5]. The volume and density were calculated using the following equations (see the Table 1 sketch for dimension nomenclature).

Top subassembly fiberboard volume,

$$V_U = (UD1)^2 (UH1) (\pi/4) + [(UD1) - 2 (UR2)]^2 (UH2) (\pi/4) - (UD2)^2 (UH3) (\pi/4) - 59.96 \text{ inch}^3$$

Top subassembly fiberboard weight, W_U = upper subassembly weight – 9.773 lb

Top subassembly fiberboard density, $\rho_U = W_U / V_U$

Bottom subassembly fiberboard volume,

$$V_L = (LD1)^2 (LH1) (\pi/4) - [(LD2) + 2 (LR1)]^2 (LH3) (\pi/4) - (LD2)^2 (LH2) (\pi/4) - 59.96 \text{ inch}^3$$

Bottom subassembly fiberboard weight, W_L = bottom subassembly weight – 4.827 lb

Bottom subassembly fiberboard density, $\rho_L = W_L / V_L$

Fiberboard dimensions measured during field surveillance are summarized in Attachment 1, and are consistent with drawing requirements except where noted and destructive examination measurements. For each of the dimensions measured in both the field surveillance and destructive examination, the measured values are similar. The dimensions were measured twice in SRNL, 3 and 168 days after the field surveillance. Most of the dimensional measurements remain consistent over time. Where changes occurred, they often reflect redistribution of moisture within the fiberboard.

Two fiberboard dimensions measured during field surveillance did not meet specified criteria. The axial gap (1.659 inch) is significantly larger than the nominal value of 0.8 inch. This results primarily from moisture accumulation in the bottom fiberboard layers, which causes these layers to compress under the weight of the package internal components (shield and containment vessels) and the package contents. This is seen by comparing dimensions LH1 and LH2 in Table 1. Dimension LH1 (the full height of the lower fiberboard subassembly) is 0.757 inch below nominal, while dimension LH2 (height from the bearing plate to the lower subassembly lower step) is only 0.164 inch less than nominal. This indicates a significant reduction in height has occurred below the lower bearing plate. The second dimension that did not meet the acceptance criterion in field surveillance is a calculated dimension that indicates whether an unacceptable gap exists between the upper and lower fiberboard subassemblies for any combination of dimension tolerances. However, actual dimensions of the shield and fiberboard indicate this was

not the case for this package. The combined height of the shield and lid is 25.188 inches maximum, and the combined fiberboard height between the bearing plates is 25.202 inches minimum. No fiberboard gap will result from these dimensions.

Fiberboard visual appearance:

The field surveillance report included two observations on the fiberboard appearance, noting evidence of water stains on the upper subassembly and mold on ¼ of the upper subassembly outer circumference. When first examined in SRNL, the stains were attributed to smeared glue, and the mold on the upper subassembly was also observed on adjacent regions of the drum and lower subassembly (Figures 1, 2). In addition, significant mold was observed around the bottom ~ 2 inches of the lower fiberboard subassembly and in several regions on the side (Figure 3). The bottom layers of the lower subassembly were saturated with water (darkened) and very soft. They tended to separate and split apart during handling. During the second examination in SRNL, the moisture content near the bottom was reduced, resulting in some cracking / splitting of the fiberboard (Figure 4).

Despite the high moisture concentration at the bottom of the fiberboard, gaps existed between the lower fiberboard subassembly and drum, and the lower subassembly came out smoothly without interference.

Fiberboard moisture content:

The moisture content of the fiberboard will affect its properties, including density, mechanical strength and thermal properties. Measuring the moisture content of the top and bottom subassemblies, and the relative humidity inside the package, provides reference data to potentially correlate laboratory test results with behavior in KAC. The fiberboard moisture content was measured during both of the SRNL examinations. Measurements were also taken during field surveillance to the extent the fiberboard was accessible.

A GE Protimeter Surveymaster moisture probe was used to measure the moisture content of the top and bottom fiberboard subassemblies. This probe identifies the wood moisture equivalent (WME), or the weight % of moisture that would produce the same electrical conductivity in wood. Moisture content data from each examination are presented in Figure 5.

Moisture measurements were compared to those taken during previous destructive examinations. Based on the overall average moisture content, the upper fiberboard subassembly has slightly more moisture, while the lower subassembly has significantly more moisture, compared to previous DE packages.

A relatively large moisture gradient was observed across the fiberboard side wall, as would be expected for the relatively high heat load in this package. The gradient was 9.8 %WME for the upper subassembly and 10.7 %WME for the lower subassembly 3 days after opening the package. At the time of the final examination (168 days after opening) the gradients were reduced to 3.7 and 3.0 %WME, respectively. This is consistent with previous observations that show the moisture gradient is slow to disappear after the internal heat load is removed.

Consistent with recent efforts to correlate moisture content of fiberboard with humidity in the surrounding air, data were taken to correlate these two parameters. The fiberboard was placed back in the drum with a narrow channel cut down the side. A humidity probe was placed in this channel such that it could be raised and lowered with the drum closed. The edge of the drum lid was taped to seal around the gap created by the humidity probe cable. After allowing time for the humidity levels in the drum to approach equilibrium, humidity readings were taken at several elevations along the fiberboard, and the fiberboard was then removed to measure the moisture content at those same locations. The humidity data were then converted to the relative humidity that would result from a constant temperature of 21 °C, since relative humidity is temperature dependent. These data are summarized in Figure 6, and compared to similar data from several previous DE packages and laboratory samples with cane fiberboard. The data from 9975-02101 are consistent with that from the other DE packages, and slightly lower than the laboratory data, suggesting the data from full packages was not quite at equilibrium.

Fiberboard thermal and mechanical properties:

Samples of fiberboard were removed from the bottom fiberboard subassembly to measure compressive strength, specific heat capacity and thermal conductivity. The source locations of these samples are illustrated in Figure 7. The thermal conductivity sample from the bottom center of the subassembly is oriented for heat flow in the axial direction (perpendicular to the glue joints). The thermal conductivity sample from the side is oriented for heat flow in the radial direction (parallel to the glue joints). Testing on each sample was performed at a nominal (mean) temperature of approximately 25ºC (77ºF), with no environmental conditioning. Physical data on the fiberboard samples are recorded in Table 2.

A total of four samples were prepared from the side and base of the lower subassembly for measuring the specific heat capacity of the fiberboard. The specific heat capacity was calculated in accordance with ASTM C351 at a mean temperature of ~25ºC (77ºF). This ASTM Standard specifies test temperatures that would produce a mean test temperature of 60ºC, but allows alternate test temperatures to be substituted as needed. Data were collected for a sample target temperature of 45ºC, and a water temperature of ~5ºC. The sample moisture content was 8.0 – 9.5 %WME (wood moisture equivalent). Each sample was tested four times, and all results were averaged. The average specific heat capacity value was 1336 J/kg-K. Multiplying this value by the density of the lower subassembly (291 kg/m^3) gives a heat capacity of 330,700 J/m^3-K (4.93 Btu/ft^3-F). This meets the required minimum value of 3 Btu/ft^3-F. The specific heat capacity value is within the range for typical baseline laboratory data, and is consistent with previous DE packages.

The thermal conductivity of the fiberboard was measured with either a Lasercomp Inc. Fox 300 or Fox 314 thermal conductivity instrument at a mean temperature of 25ºC (77ºF). For the sample with axial heat flow (perpendicular to the fiberboard layers), the measured thermal conductivity is 0.0662 W/m-K (0.0382 Btu/hr-ft-ºF) with a moisture content of 10.6 %WME. This value falls within the identified range [5], and is slightly higher than typical baseline laboratory data [10]. The axial thermal conductivity was also measured twice with higher moisture content (18.6 and 21.0 %WME). At these higher moisture levels, the thermal

conductivity was above the identified acceptance range. It is seen from these tests that the fiberboard density and thermal conductivity vary linearly with moisture content (Figure 8). For the sample with radial heat flow (parallel to the fiberboard layers), the measured thermal conductivity is 0.1152 W/m-K (0.0666 Btu/hr-ft-^{o}F), with a typical moisture content of 9.8 %WME. This thermal conductivity value falls within the identified range [5], and is also slightly higher than typical baseline laboratory data [10].

The compression test data are shown in Figures 9 and 10, along with baseline data for a different fiberboard assembly. A series of photographs showing typical compression behavior under parallel loading is shown in Figure 11. The area under the stress-strain curve up to 40% strain is used as a relative indication of the energy absorption capacity of the fiberboard. This metric is shown in Figure 12 for all destructively examined packages as a function of fiberboard moisture content. In general, the energy absorption capacity decreases as the moisture content increases. The results from 9975-02101 are circled in Figure 12. Based on the comparison in Figures 8 and 10, the 9975-02101 fiberboard has slightly less energy absorption capacity than the baseline samples. However, the Figure 12 data collectively show a trend consistent with the other DE packages.

Due to the high moisture levels and heavy mold around the outside bottom of the lower fiberboard subassembly, which are significantly reduced toward the package centerline, the axial thermal conductivity sample was intentionally made larger than usual. This allowed it to be further sectioned into additional compression samples after thermal conductivity testing was completed. The relative position of each of these samples was tracked to identify the distance from it to the package centerline. After allowing these samples to dry to a uniform moisture content (~11 – 13 %WME), these samples were tested to identify whether the elevated moisture and/or mold had created a permanent decrease in density or strength. By performing this exercise on samples that were removed from the same fiberboard layers with a similar moisture content, much of the potential for sample-to-sample variation is eliminated. Results are summarized in Figures 12 and 13. A pronounced decrease in density (up to 10%) is seen for samples more than ~5 inches from the centerline. Energy absorption (represented by the area under the stress-strain curve up to 40% strain) also shows a decrease in this region up to ~25%. While there is variation in these data, some of the samples from the outer molded region (more that ~5 inches from the centerline), are seen in Figure 12 to fall slightly below the envelope of other DE packages. This indicates that the fiberboard was degraded locally in its properties from the elevated moisture and/or mold.

Data from the primary compression samples removed from the base layers (and tested at 24 %WME) are also shown in Figure 13 for comparison. The higher moisture content increases the density, and decreases the energy absorption. For perpendicular orientation samples, the energy absorption is barely above the 11 psi limit based on the forklift impact scenario. While this heavily degraded condition exists only in a small region of the lower fiberboard assembly, it illustrates that moisture and mold have the potential to produce significant degradation in properties. Note, however, that the fiberboard properties away from this limited region are consistent with that typically seen in other non-degraded packages.

Lead shield examination:

The entire surface of the lead shield was visually examined. It was found to be free from significant deformation and physical damage. The outer side surface is covered with white corrosion product, with varying thickness, as has been observed on other packages (Figure 14).

Several lead shield dimensions were measured (Table 3) and all but one are consistent with drawing requirements. The inside diameter at the top was slightly greater than specified (7.267 inches vs 7.26 inches maximum).

The radial thickness was measured near the top of the shield, and was calculated from diametral data taken near the bottom of the shield. The calculated thickness from near the bottom (0.538 inch) is similar to the measured thickness near the top (0.544 inch). This comparison is made to indicate whether the lead may have undergone creep during service; and indicates no significant creep has occurred to date.

O-ring examination and testing:

Prior surveillance testing of the four O-rings from this package included visual examination, dimensional and hardness measurements. Dimensional measurements were repeated on each O-ring as part of the destructive examination. Three of these O-rings (SCV outer, PCV outer and PCV inner) received additional testing. All three were submitted for FT-IR spectroscopy to confirm material composition, and the two outer O-rings received optical and SEM microscopic examination of the cross section. The dimensions and weight of the SCV outer and PCV outer O-rings were recorded to calculate their density. The PCV inner O-ring was tensile tested, including a hold point at 50% strain to visually examine the O-ring.

Weight and dimension data for the two outer O-rings are presented in Table 4. The average minor diameter for each O-ring is within the specified tolerances for new O-rings, but the major inside diameter for each O-ring (calculated from the length measured after the O-ring was cut) is greater than specified for new O-rings. This is consistent with a permanent stretch due to the lid diameter. Leak testing during the field surveillance successfully demonstrated leak-tightness to a level of approximately 1×10^{-3} std cc air/sec.

Compression set was calculated for each O-ring based on each of the dimensional measurements it received. Compression set is calculated as follows, assuming an initial minor diameter of 0.139 inch and an average groove depth in the lid of 0.0995 inch.

$$\text{Compression set (\%)} = (0.139 - \text{radial thickness}) / (0.139 - 0.0995)*100$$

Compression set for the 9975-02101 O-rings ranged from 2 to 38% based on KAC measurements. For the smaller of these values, individual readings varied significantly, suggesting the O-ring had twisted after removal. The compression set decreases with time, as the polymer continues to relax. Typically, the compression set has reached an equilibrium value after about 30 days. When measured in SRNL 188 days later, the compression set ranged from 2

to 10%. The compression set values are generally consistent with the range of values measured for O-rings from other packages.

FT-IR spectroscopy generically identified the composition of each O-ring as consistent with a Viton® type fluoroelastomer (Figure 15). Each O-ring produced a similar FTIR spectrum consistent with that from previous characterization of Viton® GLT O-rings, and with a library image of a Viton® FTIR spectrum.

As with previous destructive examinations, visual (Figure 16) and SEM (Figure 17) examination of the cross sections identified a distribution of very small particles throughout each O-ring. Aside from carbon and fluorine (the primary constituents of Viton® fluoroelastomer) the SEM identified small amounts of zinc, aluminum, silicon, sulfur, calcium, and oxygen. Though the actual compound is proprietary, Viton®-type fluoroelastomer compounds typically contain MgO, CaO, $Ca(OH)_2$, ZnO or lead compounds as acid acceptors and heat stabilizers [11]. Aluminum is present in hydrotalcite, which is used in both GLT and GLT-S compounds as a filler reinforcing agent. Silicon may be present as a trace contaminant.

The PCV inner O-ring was tensile tested in accordance with ASTM D1414, using a cut (single strand) sample. The test was interrupted at 50% strain (Figure 18) to visually examine the O-ring for signs of cracking or other degradation. None were observed. The initial stress-strain curve for the PCV inner O-ring is shown in Figure 19, along with results of other tests with Viton GLT O-rings. In this first test, the O-ring failed after reaching 356% elongation. A re-test was performed with a different grip arrangement, and reached 285% elongation (Figure 20). The first test uses a yarn grip which would allow some stretch beyond the gage section, especially if the O-ring had any residual grease. To more accurately measure the elongation, the second test was performed with an alternate grip arrangement which does not allow such stretch. Since these alternate flat grips pose a greater risk of breaking within the grips (which would invalidate the test), the portion of O-ring within the grips was wrapped with tape for cushioning.

General:

A general visual examination was performed on all metallic components. No significant damage or degradation of the containment vessels was observed. Various fabrication markings were stamped or engraved on the containment vessels and lids. These markings appear to be identification numbers used during manufacture, prior to association of the parts with a final package number, and are consistent with those seen in other packages.

Corrosion was observed in four areas around the bottom edge of the drum exterior (Figure 21). Figure 22 shows corrosion on the inner drum surface just above the bottom crevice opposite three of these locations. The third of these locations is shown in Figure 23 after light cleaning. A small amount of water was placed in the drum, with the drum tipped slightly to concentrate the water at one of these corrosion locations. Water was later observed on the outside at that location, demonstrating a leak path through the bottom joint of the drum exists. It is anticipated that this leak path existed originally, and that the corrosion may have exacerbated that condition. Corrosion was also observed along the corner on the bottom of the drum (Figure 24). A section

of the bottom edge was removed for metallographic examination that included the corrosion shown in Figure 21(c) and some of the corrosion on the drum bottom (Figure 25).

Figure 26 shows a cross section through the drum bottom flange less than ½ inch from one of the corroded locations, for reference. Limited corrosion was noted at this location slightly higher up on the drum exterior side. In comparison, Figure 27 shows a cross section through the primary area of attack, with general/pitting corrosion as well as cracking. The general/pitting corrosion is heaviest in the weld metal. Both corrosion and cracking are seen to extend through a single wall thickness in this cross section. However, it is judged that the overall integrity of the drum with regards to performing its safety function is still adequate. The impact of these observations in under evaluation.

When corrosion has been observed on the drum from other 9975 packages, it is typically heaviest along the bottom edge at the ends of the stitch welds. Two reasons contribute to this behavior. First, the residual stresses from these welds are prone to create larger gaps between the interlocking layers in the bottom edge. With the larger gaps, leakage through these local areas will increase and chlorides and other corrosive constituents that might leach from the fiberboard can preferentially concentrate at these locations. Second, the typical weld filler metal used on stainless steel is prone to contain elevated levels of ferritic microstructure, which can be more susceptible to corrosion. However, it is noted that corrosion has also been observed on the bottom surface of 9975 drums, and adjacent to the side seam weld [7, 12]. Neither of these locations is associated with a direct leak path or ferritic microstructure. Therefore, any change to the stitch weld configuration may reduce the severity of corrosion, but is not likely to eliminate it.

The data from the examination activities described above are compared with field surveillance data in Attachment 1. There is general agreement between the two examinations, although some differences are to be expected as moisture re-distributes within the fiberboard and the O-rings slowly relax. All findings will be reviewed by NMM for potential impact on the continued storage of other packages in KAC.

Measurement Uncertainties:

Numerous measurements were made with a variety of instruments during the destructive examination of package 9975-02021. Some of the measurements were specifically compared to inspection criteria, while others were taken for information / trending purposes. All measurements which are compared to inspection criteria were made with calibrated instruments, or were verified against calibrated instruments. The uncertainties associated with measurements and calculated results required to meet inspection criteria are discussed below.

Weight – The weight of each fiberboard subassembly was measured to a precision of 1 gram. The balance used was M&TE, and the calibration data show accuracy within 5 grams over the range of interest. A conservative net uncertainty of 6 grams will be used.

Calipers – Three different calipers were used to measure component dimensions. All three calipers are M&TE, and calibration data show accuracy within 0.001 inch. In addition, operator

bias can affect measurement accuracy through the contact load applied when making a measurement. A degree of give exhibited by the fiberboard will lead to different results as the contact load changes. The larger calipers are judged to be more susceptible to this bias. Metallic components are significantly more rigid than the fiberboard, but operator bias may also exist for those components. While not characterized explicitly, it is judged that the total uncertainty (instrument uncertainty plus operator bias) for fiberboard measurements is no greater than +/- 0.003 inch for the 6 inch calipers, +/- 0.005 inch for the 24 inch calipers, and +/- 0.007 inch for the 40 inch calipers. It is further judged that total uncertainty when measuring metallic components is no greater than +/- 0.003 inch for 6 and 24 inch calipers, and +/- 0.005 inch for the 40 inch calipers.

Manual calipers – Dimension ID2 on the lead shield was captured with manual swing calipers, which was then locked in that position and measured with 24-inch calipers. It is judged that the accuracy of capturing this dimension with the manual calipers is within +/- 0.002 inch, and the measurement of that dimension is then within +/- 0.002 inch, for a (conservatively) combined accuracy of +/- 0.004 inch.

Thermal conductivity instrument – The specifications for the Fox300 and Fox 314 thermal conductivity instruments include a stated accuracy of ~1% and 2%, respectively. Measurement of the thermal conductivity of a calibration standard was accurate to within 1.1% on either instrument. Prior test reports of fiberboard samples from an independent laboratory, using a Fox 300 instrument, identified an overall 3% uncertainty. An uncertainty of 3% will be conservatively assumed for the current measurements.

Heat capacity – The specific heat capacity is derived from temperature and weight measurements, using calibrated instruments. The thermocouple and balance precisions are high. The greatest contribution to error in the specific heat capacity is considered to be consistency of operator technique. The total uncertainty is reflected in the range of results for multiple trials. The heat capacity was measured four times on each of four samples. The variation for each sample ranged from 24 to 44%. The combined uncertainty on the average of 4 samples is 18%.

Where measurement results are used in subsequent calculations, the uncertainty values identified above are assumed to be random. A standard error propagation formula for random errors is used to calculate the final result uncertainty. In some cases, the calculated uncertainty may be less than the potential error from rounding off the result, and the higher variation associated with round-off is reported as the uncertainty. These calculations are documented in the Laboratory Notebook [9]. Calculation results and their uncertainties are summarized as follows:

- Top fiberboard subassembly volume = 28297 +/- 26 cm^3
- Top fiberboard subassembly density = 0.264 +/- 0.001 g/ cm^3
- Bottom fiberboard subassembly volume = 83165 +/- 71 cm^3
- Bottom fiberboard subassembly density = 0.291 +/- 0.001 g/ cm^3
- Shield radial thickness at bottom = 0.538 +/- 0.003 inch
- Thermal conductivity (radial) = 0.0666 +/- 0.002 Btu/hr-ft-ºF
- Thermal conductivity (axial) = 0.0382 +/- 0.001 Btu/hr-ft-ºF
- Heat capacity = 4.9 +/- 0.9 Btu/ft^3-ºF

References

[1] WSRC-SA-2002-00005, Rev. 10, "K-Area Material Storage Facility Documented Safety Analysis", October 2014.

[2] SRNS-STI-2010-00763 Rev. 0, "9975 Shipping Package Life Extension Surveillance Program Results Summary", W. L. Daugherty, K. A. Dunn, E. R. Hackney, E. N. Hoffman and T. E. Skidmore, January 2011.

[3] SFS-ENG-99-0085, "Summary and Guide to 9975 Container Qualification Program"

[4] WSRC-TR-2001-0286, Rev. 4, "The Savannah River Site Surveillance Program for the Storage of 9975/3013 Plutonium Packages in KAC", July 2008

[5] WSRC-TR-2005-00135 Rev. 1, "Task Technical and Quality Assurance Plan for Destructive Examination of a 9975 Package from Field Surveillance Activities", W. L. Daugherty, March 2011

[6] WSRC-TR-2004-00197, "Inspection Activities and Acceptance Criteria for Field Surveillance of Model 9975 Package O-Rings and Celotex® Materials", W. L. Daugherty, April 2004

[7] SRNL-STI-2016-00014, "Examination of Shipping Packages 9975-01641, 9975-01692, 9975-03373, 9975-02101 and 9975-02713", W. L. Daugherty, January 2016

[8] SOP-CSS-207-K, Rev. 9, Attachment 2 "9975 Surveillance Data Sheet" for 9975-02101

[9] SRNL-NB-2012-00048, Laboratory Notebook "9975 Shipping Package Celotex Testing Book IV

[10] SRNL-STI-2015-00610, "Status Report – Cane Fiberboard Properties and Degradation Rates for Storage of the 9975 Shipping Package in KAC", W. L. Daugherty, December 2015

[11] Rubber Technology Handbook, W. Hofmann, Hanser Publishers, New York, 1989, page 122

[12] SRNL-STI-2016-00152, "Examination of Shipping Package 9975-02403", W. L. Daugherty, March 2016

Table 1. Fiberboard physical measurements and calculated density

Upper Subassembly						
Weight	11.906 kg					R-R2-F-0019 Rev 5
	0/180 deg.		90/270 deg.		Avg.	Nominal value (inch)
UD1 (in)	17.626		17.655		17.640	17.7
UD2 (in)	8.580		8.582		8.581	8.55
	0 deg.	90 deg.	180 deg.	270 deg.	Avg.	
UR1 (in)	3.040	3.062	3.068	3.038	3.052	3.075
UR2 (in)	1.455	1.433	1.482	1.491	1.465	1.5
UH1 (in)	7.074	7.021	7.050	7.056	7.058*	7.1
UH2 (in)	2.064	2.077	2.092	2.052	2.071	2.1
UH3 (in)	5.002	4.971	4.980	4.980	4.983	5.0

* UH1 average value is adjusted by 0.008 inch to account for fiberboard that remained stuck to the air shield.
Upper subassembly calculated density = 0.264 g/cc

Lower Subassembly						
Weight	26.417 kg					R-R2-F-0019 Rev 5
	0/180 deg.		90/270 deg.		Avg.	Nominal value (inch)
LD1 (in)	18.050		18.048		18.049	18.1
LD2 (in)	8.482		8.480		8.481	8.45
	0 deg.	90 deg.	180 deg.	270 deg.	Avg.	
LR1 (in)	3.309	3.284	3.260	3.290	3.286	3.275
LR2 (in)	1.494	1.498	1.493	1.491	1.494	1.55
LH1 (in)	25.872	25.954	26.026	25.919	25.943	26.7
LH2 (in)	20.231	20.249	20.234	20.232	20.236	20.4
LH3 (in)	2.006	2.007	2.015	2.050	2.020	2.0

Lower subassembly calculated density = 0.291 g/cc

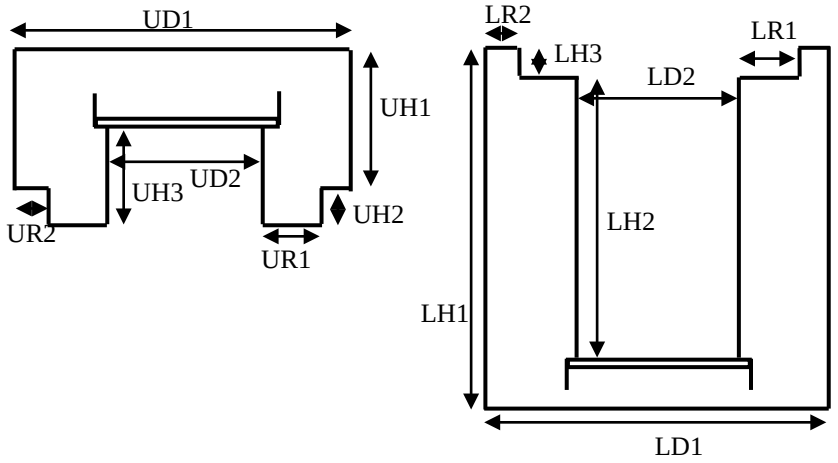

Table 2. Physical data for fiberboard test specimens

Test Sample	Moisture Content (%WME)	Weight (g)	Length (inch)	Width (inch)	Height (inch)	Density (g/cc)
Compression Test Samples						
Side 1 (parallel)	9.0	37.073	2.045	2.050	2.035	0.265
Side 2 (parallel)	9.0	39.829	2.048	2.051	2.039	0.284
Side 3 (perpendicular)	9.3	40.712	2.054	2.067	2.033	0.288
Side 4 (perpendicular)	9.2	39.643	2.053	2.068	2.037	0.280
Base 1 (parallel)	24.0	38.477	2.018	2.021	2.026	0.284
Base 2 (parallel)	24.0	38.125	2.024	2.022	2.014	0.282
Base 3 (perpendicular)	24.3	38.072	2.022	2.024	2.015	0.282
Base 4 (perpendicular)	24.5	38.913	2.023	2.026	2.042	0.284
Thermal Conductivity Samples						
Side (radial)	9.8	376	7.010	6.980	1.673	0.280
Base (axial) *	21.0 10.6	975 929	11.581 11.560	8.470 8.442	2.066 2.035	0.294 0.285

Data provided for the axial thermal conductivity as-sectioned, and after drying to a “typical” level.

Table 3. Lead shield dimensions

Dimension	0/180 deg. (inch)		90/270 deg. (inch)		Avg. (inch)	Requirement (inch)
OD (in)	8.330		8.327		8.328	8.252 – 8.35
ID1 (in)	7.257		7.274		7.266*	7.25 – 7.26
ID2 (in)	7.252		7.250		7.251	7.24 – 7.26
	0 deg.	90 deg.	180 deg.	270 deg.		
R (in)	0.550	0.542	0.544	0.547	0.544	0.506 min
H (in)	24.692	24.678	24.686	24.684	24.685	24.556 – 24.7

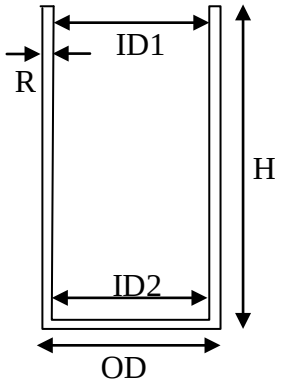

(OD – ID2) / 2 = 0.538 inch

* ID1 re-measured at 4 locations, average value = 7.267 inch

Table 4. O-ring physical data

~60 Days after Field Surveillance	PCV Outer O-Ring Thickness		SCV Outer O-Ring Thickness	
	Radial (inch)	Axial (inch)	Radial (inch)	Axial (inch)
Minor Dia. 0 deg	0.1335	0.1370	0.1350	0.1320
Minor Dia. 45 deg	0.1335	0.1365	0.1370	0.1340
Minor Dia. 90 deg	0.1365	0.1350	0.1385	0.1330
Minor Dia. 135 deg	0.1345	0.1320	0.1390	0.1305
Minor Dia. 180 deg	0.1350	0.1330	0.1355	0.1305
Minor Dia. 225 deg	0.1370	0.1335	0.1415	0.1305
Minor Dia. 270 deg	0.1390	0.1315	0.1415	0.1325
Minor Dia. 315 deg	0.1370	0.1355	0.1375	0.1315
Avg. Minor Dia.	**0.1350**		**0.1350**	
Minor Dia. (new)	0.138 +/- 0.006 inch		0.138 +/- 0.006 inch	
Length (after cut)	14 3/32 inch		17 8/32 inch	
Calculated Major Dia.	4.486 inch avg		5.491 inch avg.	
Major Inside Dia. (new)	4.234 +/- 0.030 inch		5.234 +/- 0.035 inch	
Weight	6.0144 g		7.1660 g	
Calculated Volume	0.202 $inch^3$ (3.310 cm^3)		0.247 $inch^3$ (4.046 cm^3)	
Calculated Density	**1.817 g/cm^3**		**1.771 g/cm^3**	

Figure 1. Upper fiberboard subassembly with mold and dark regions attributed to smeared glue.

Figure 2. Mold between lower fiberboard subassembly and drum, coincident with the mold on the upper fiberboard subassembly.

(a)

(b)

Figure 3. Lower fiberboard subassembly mold in the bottom saturated layers (a) and on the side (b).

Figure 4. Cracking of the lower fiberboard subassembly following partial drying out.

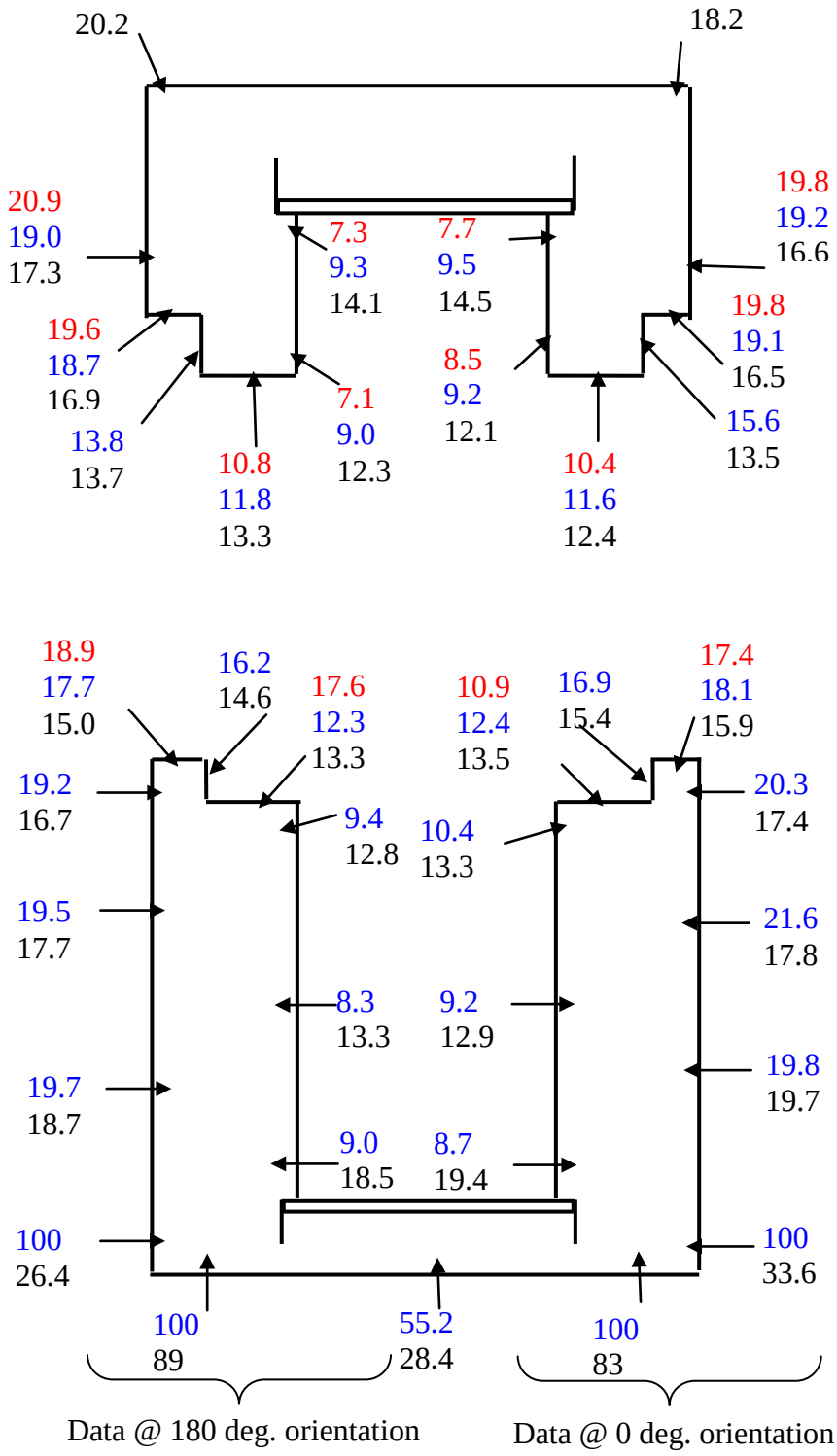

Figure 5. Fiberboard moisture content data. The values in red were measured during field surveillance. The values in blue were measured 3 days later, while the values in black were measured 168 days after field surveillance. All values are % wood moisture equivalent.

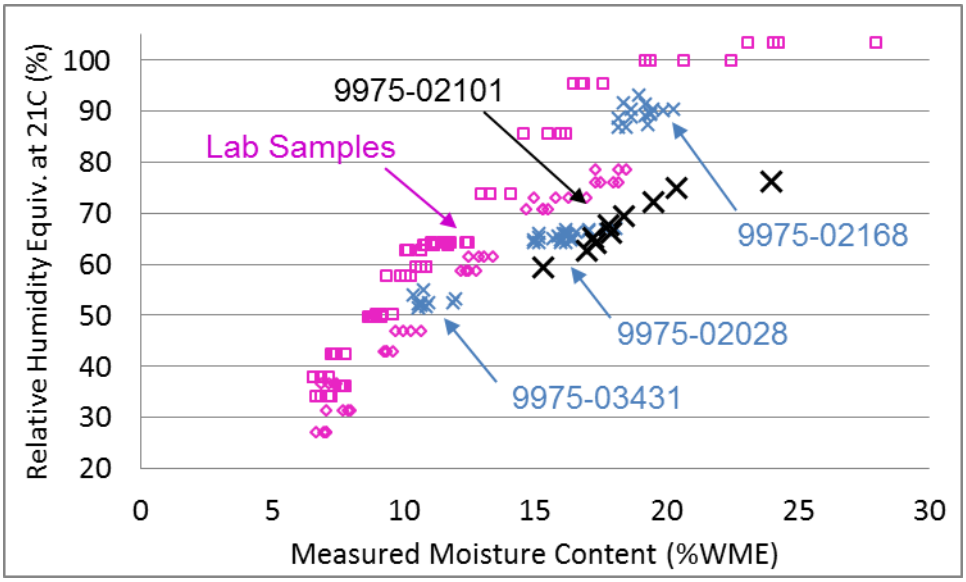

Figure 6. Correlation between fiberboard moisture content and relative humidity of the adjacent air. Data from 9975-02101 are shown with comparable data from prior cane fiberboard DE packages and laboratory samples. Measurements were taken along the fiberboard OD surface. Since relative humidity is temperature dependent, all the data in this graph have been converted to a consistent equivalent relative humidity at 21 °C.

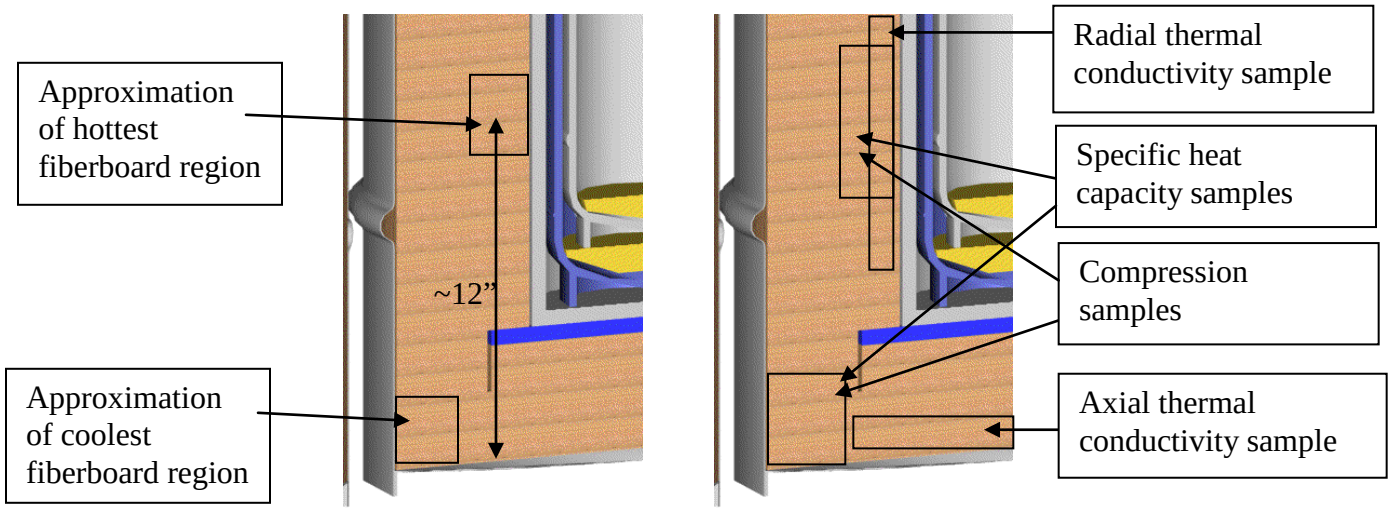

Figure 7. Illustration of fiberboard regions of the lower subassembly to be tested. Multiple samples (where used) were removed from the illustrated locations at different circumferential positions. Not to scale.

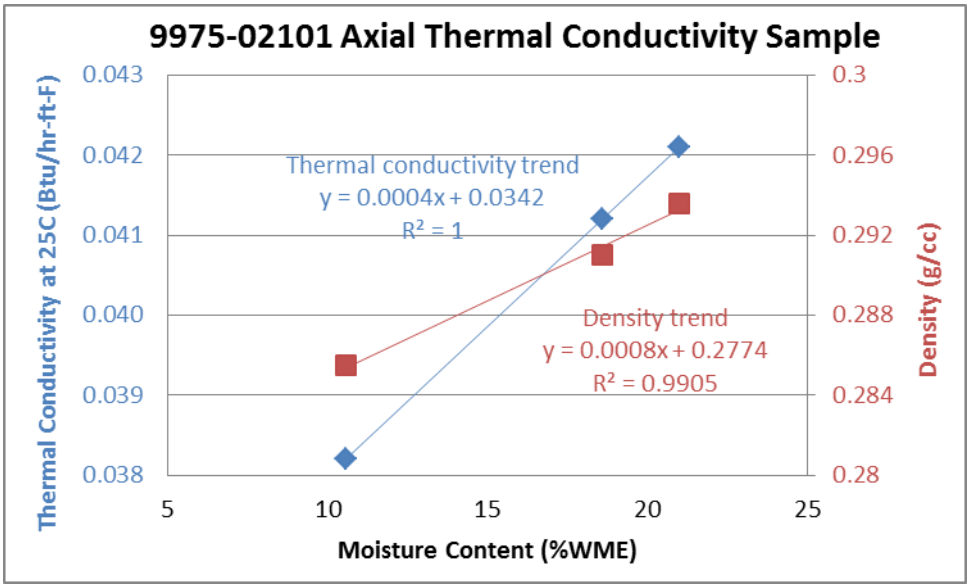

Figure 8. Variation in thermal conductivity and density as a function of fiberboard moisture.

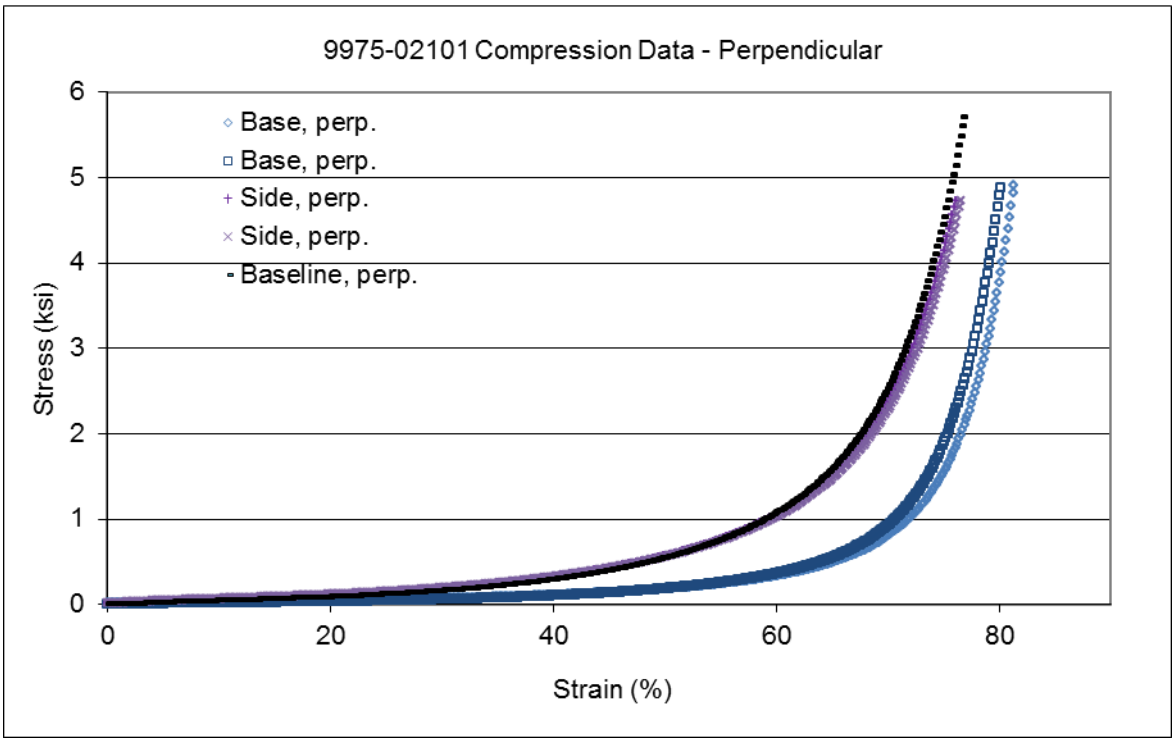

Figure 9. Fiberboard compression test data, compared with typical baseline data from an unaged assembly, in the perpendicular orientation (i.e. load applied perpendicular to the fiberboard layers).

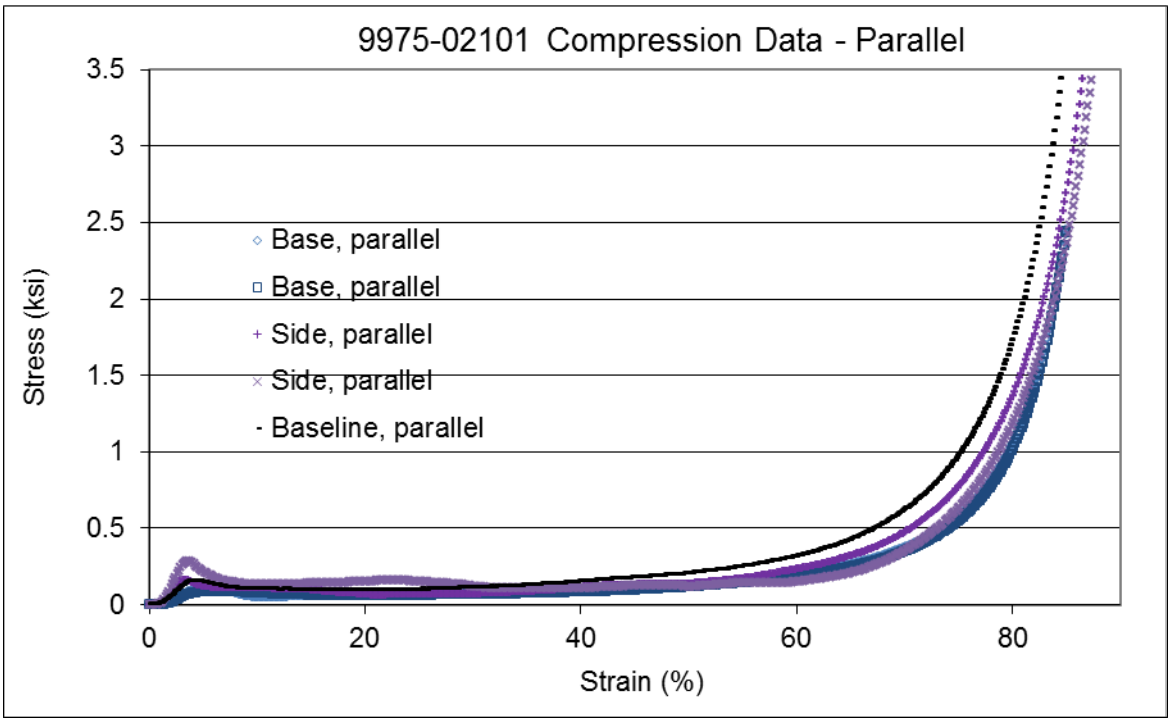

(a)

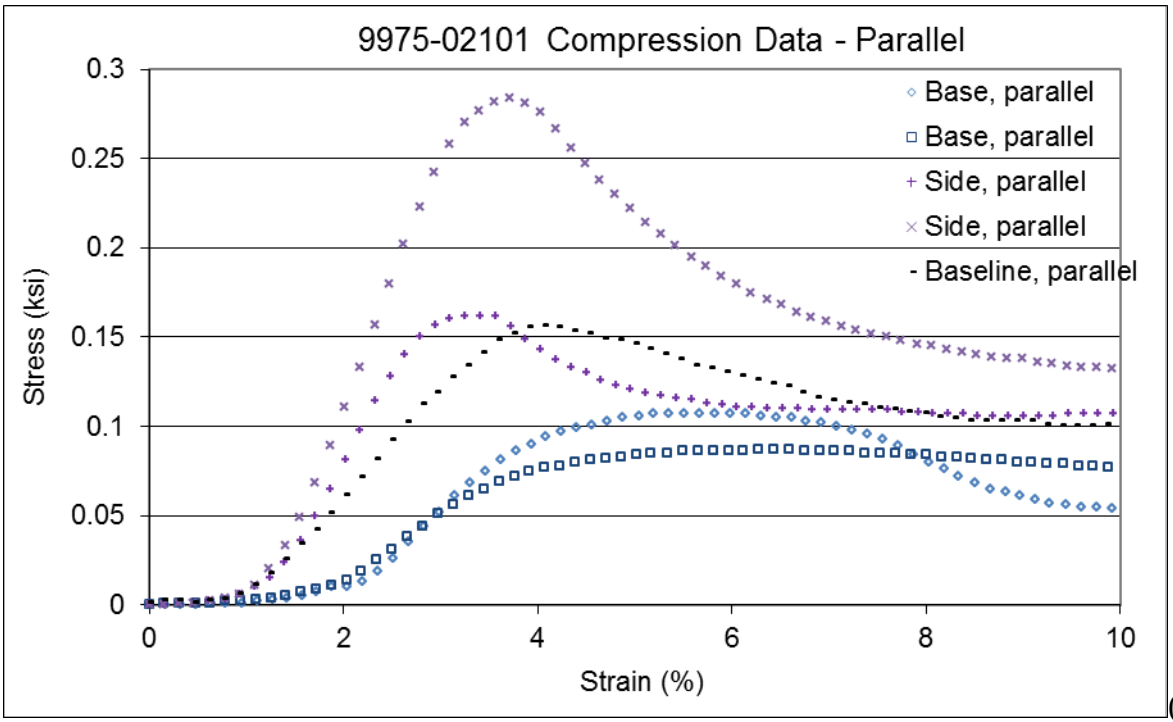

(b)

Figure 10. Fiberboard compression test data, compared with typical baseline data from an unaged assembly, in the parallel orientation (i.e. load applied parallel to the fiberboard layers). The full curves are shown in (a), while the initial buckling region is expanded in (b).

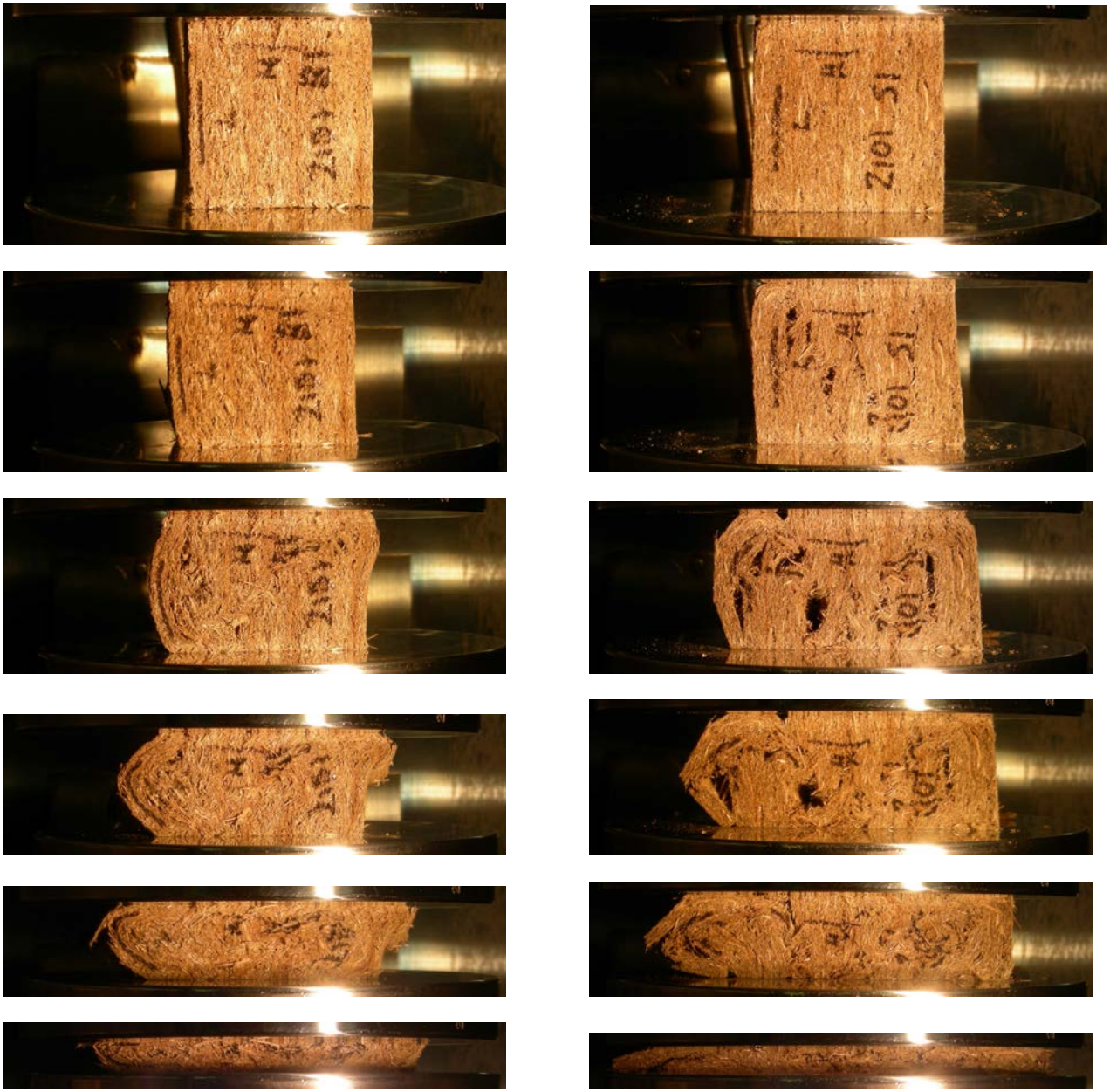

(a) Sample B1 from base of subassembly (b) Sample S1 from side of subassembly

Figure 11. Photographs of fiberboard samples during compression testing, parallel orientation

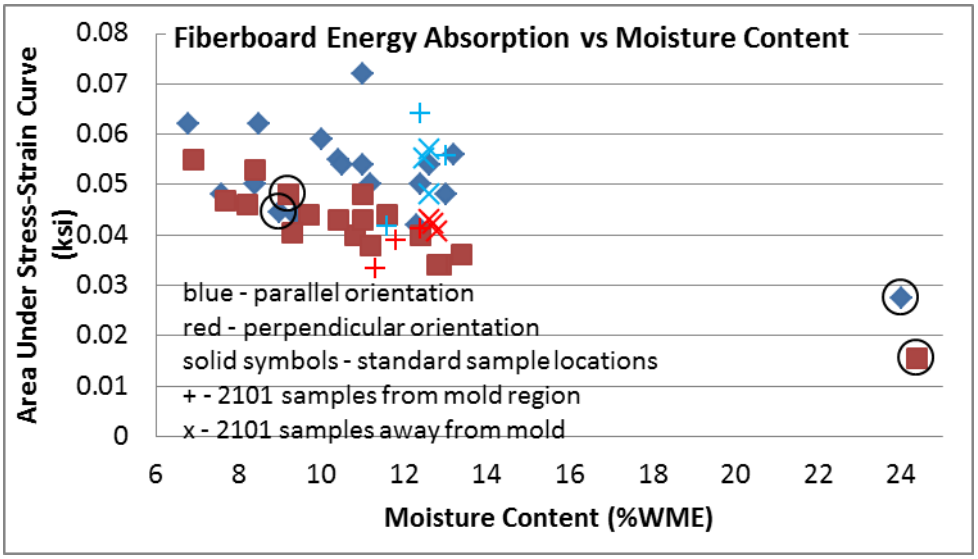

Figure 12. Fiberboard energy absorption, represented by the area under the stress-strain curve up to 40% strain, from tensile test samples from all destructively examined packages. The results from the standard locations in 9975-02101 are circled. The +, x symbols indicate additional samples from 9975-02101 base representing either the mold region (+) or away from the mold (x).

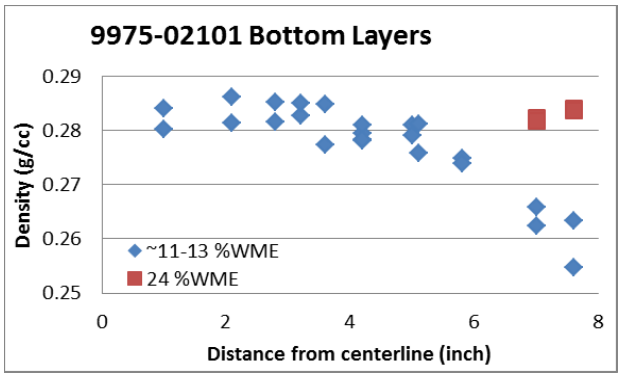

(a) Density

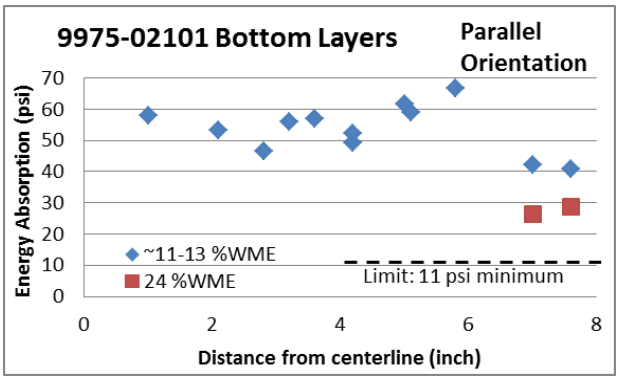

(b) Energy absorption for parallel orientation

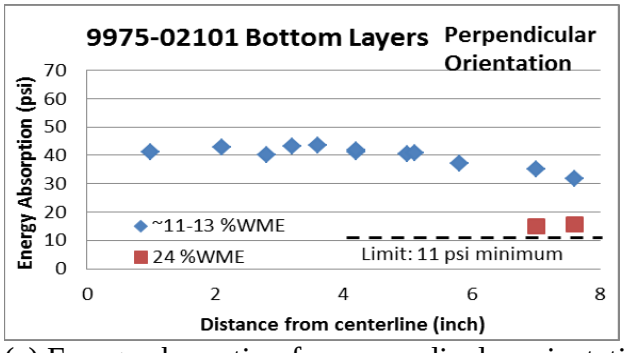

(c) Energy absorption for perpendicular orientation

Figure 13. Additional density and mechanical data from bottom fiberboard layers. Samples taken further from the package centerline had higher moisture content and more mold. These samples were dried to a more consistent 11 – 13 %WME moisture content before testing. Results for the compression samples taken from the bottom layers and tested at 24 %WME are shown for comparison.

Figure 14. Lead shield with white corrosion product.

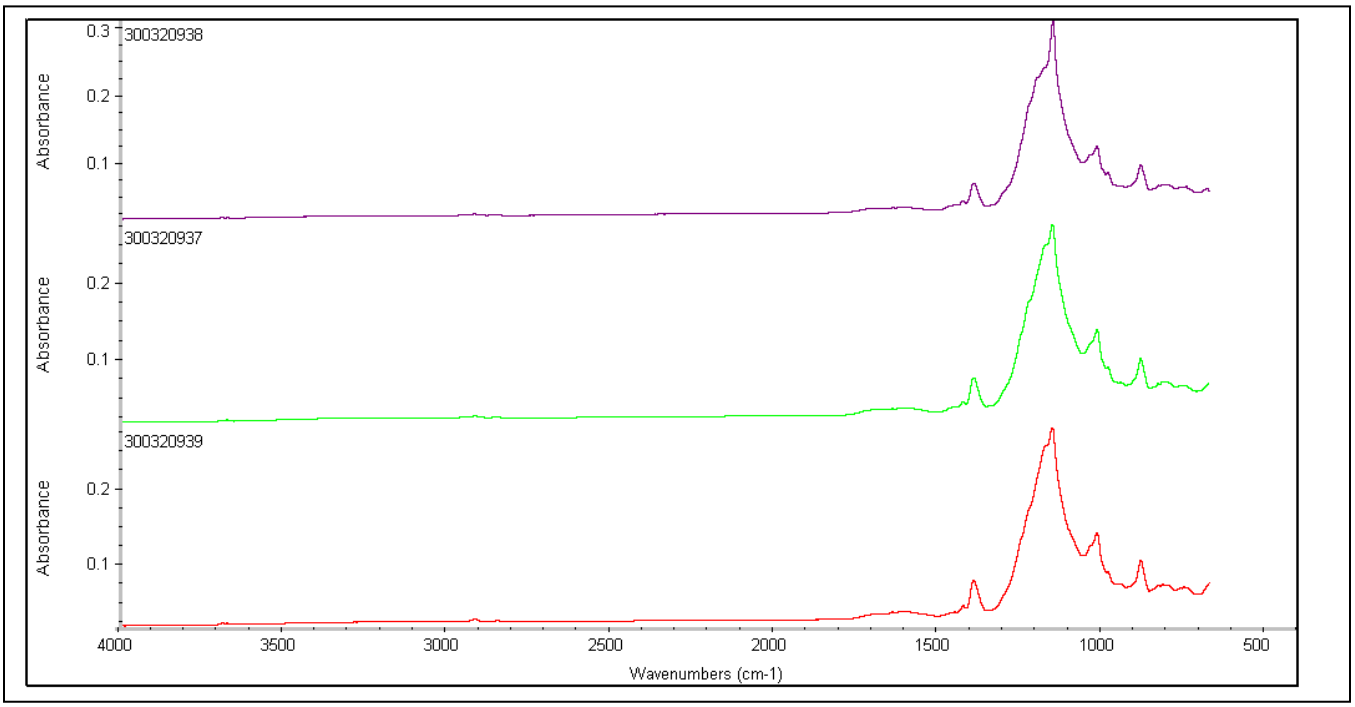

Figure 15. FT-IR spectra for the three tested Viton® GLT-S O-rings from 9975-02101. PCV outer – purple, PCV inner – green, SCV outer – red.

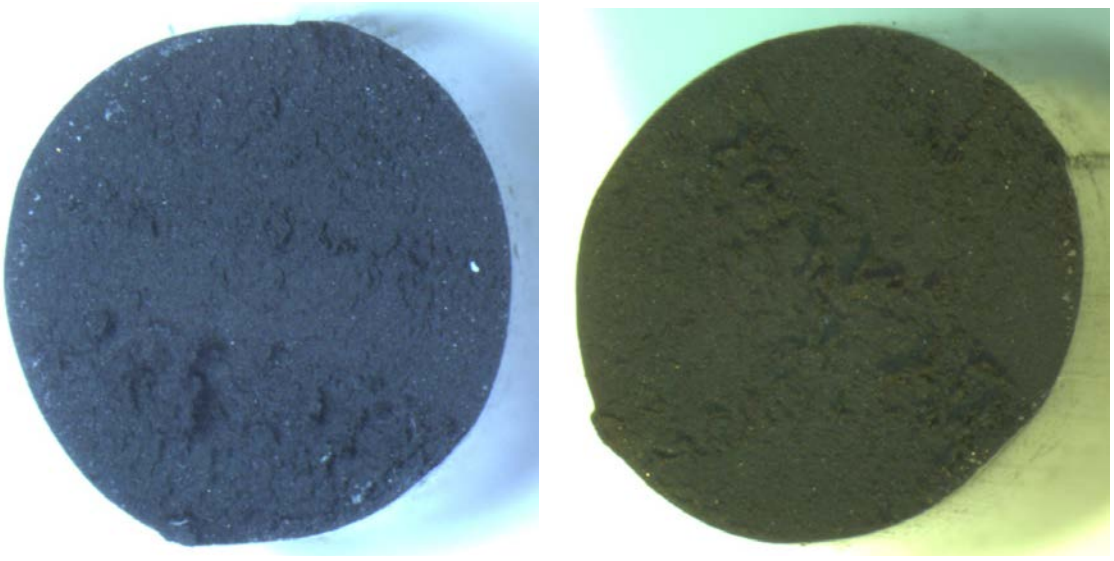

(a) (b)

Figure 16. Optical cross section of the (a) PCV outer and (b) SCV outer O-rings. Photos taken by 723-A Met Lab.

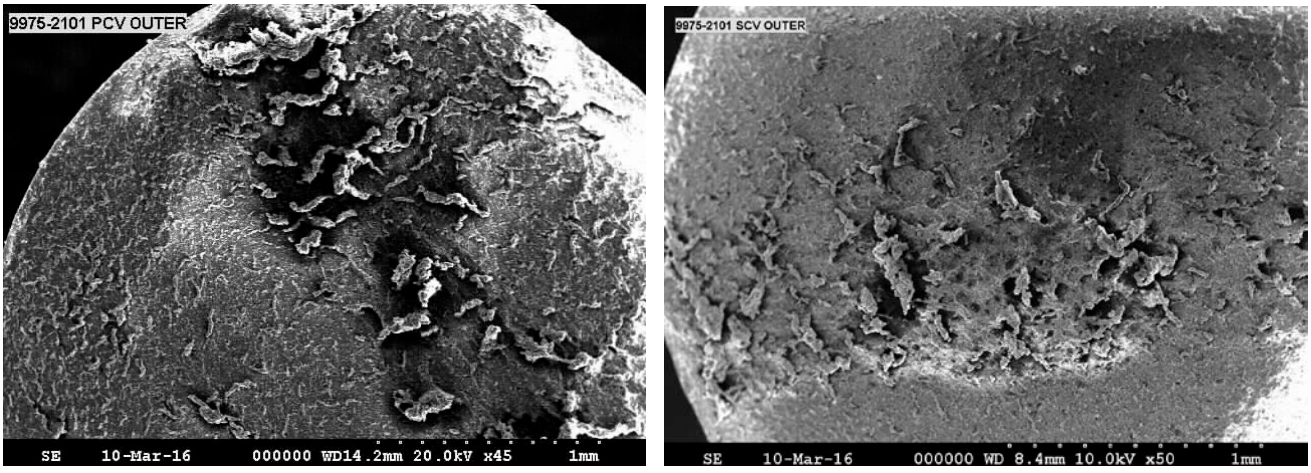

(a) (b)

Figure 17. SEM cross section of the (a) PCV outer and (b) SCV outer O-rings. Photos taken by 723-A Met Lab.

Figure 18. 9975-02101 PCV inner O-ring during tensile test, at 50% stretch.

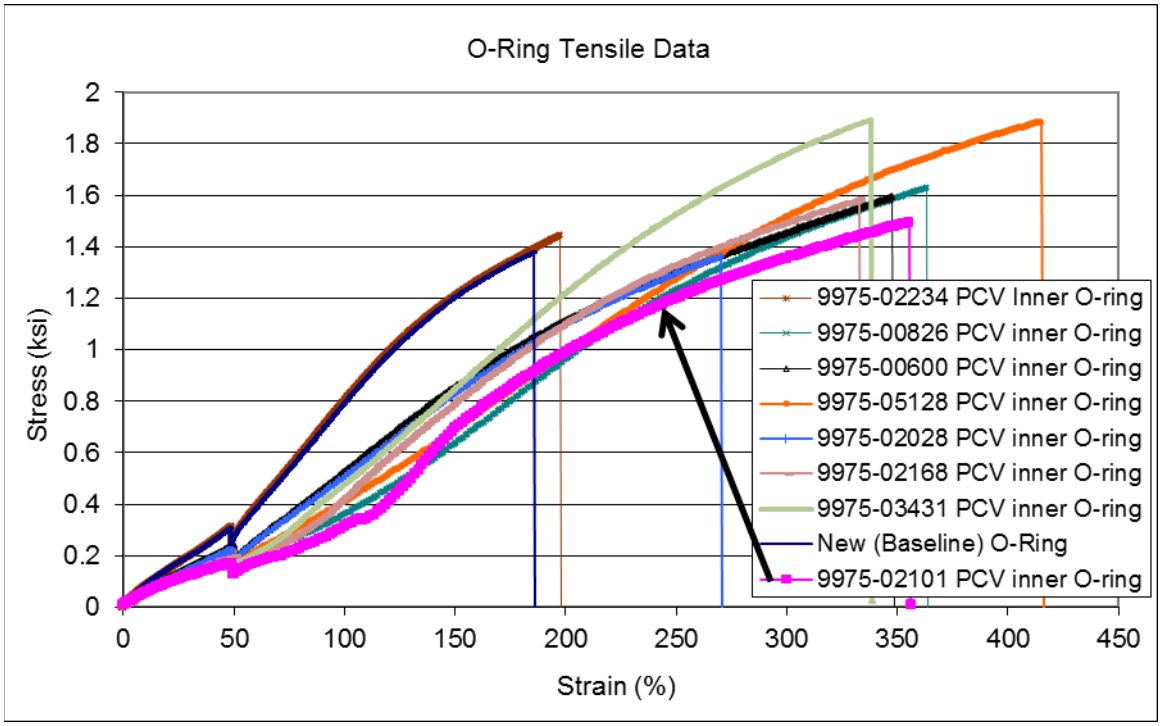

Figure 19. Tensile data for PCV inner O-ring from 9975-02101 tested with the original yarn grip configuration, with comparison curves from other DE packages.

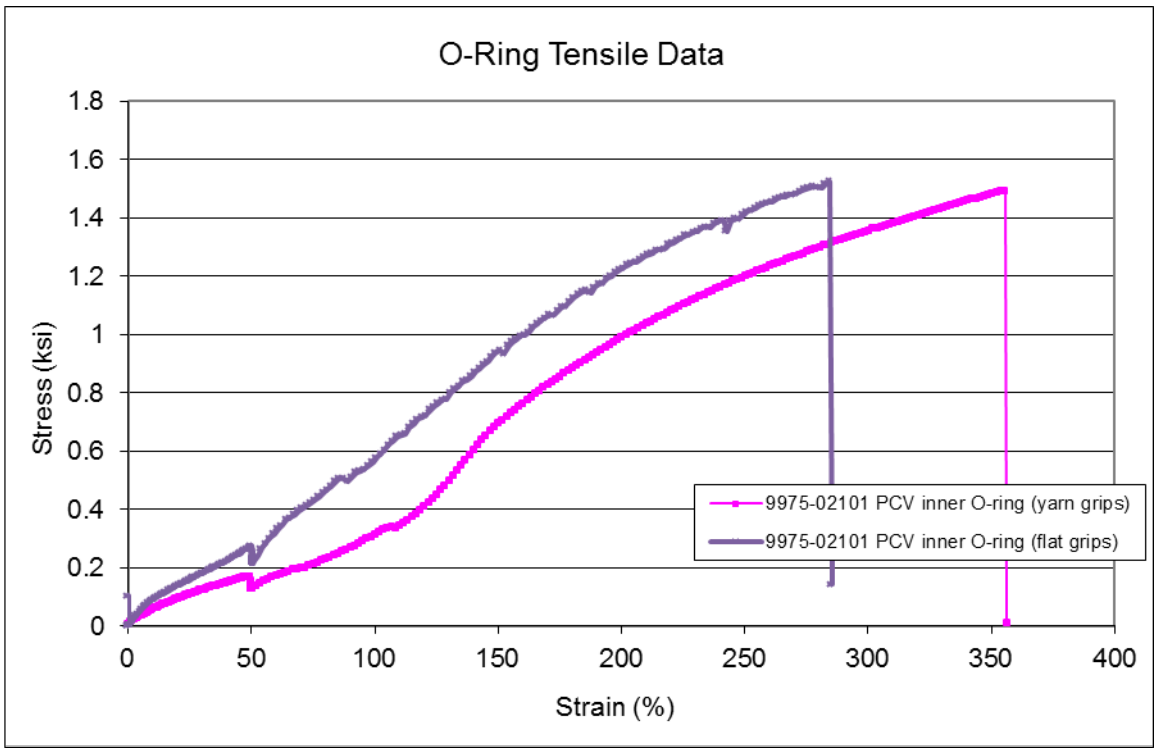

Figure 20. Tensile data for PCV inner O-ring from 9975-02101 comparing effect of yarn grips and flat grips.


(a)


(b)

(c)


(d)

Figure 21. Four areas of corrosion on the drum exterior along the bottom edge.

(a)

(b)

(c)

Figure 22. Corrosion (and fiberboard residue) on the drum interior opposite that shown in Figure 21 (a), (b) and (c).

Figure 23. Corrosion on the drum interior opposite that shown in Figure 21 (c) after light cleaning.

Figure 24. Corrosion on the bottom of the drum, along the outer corner.

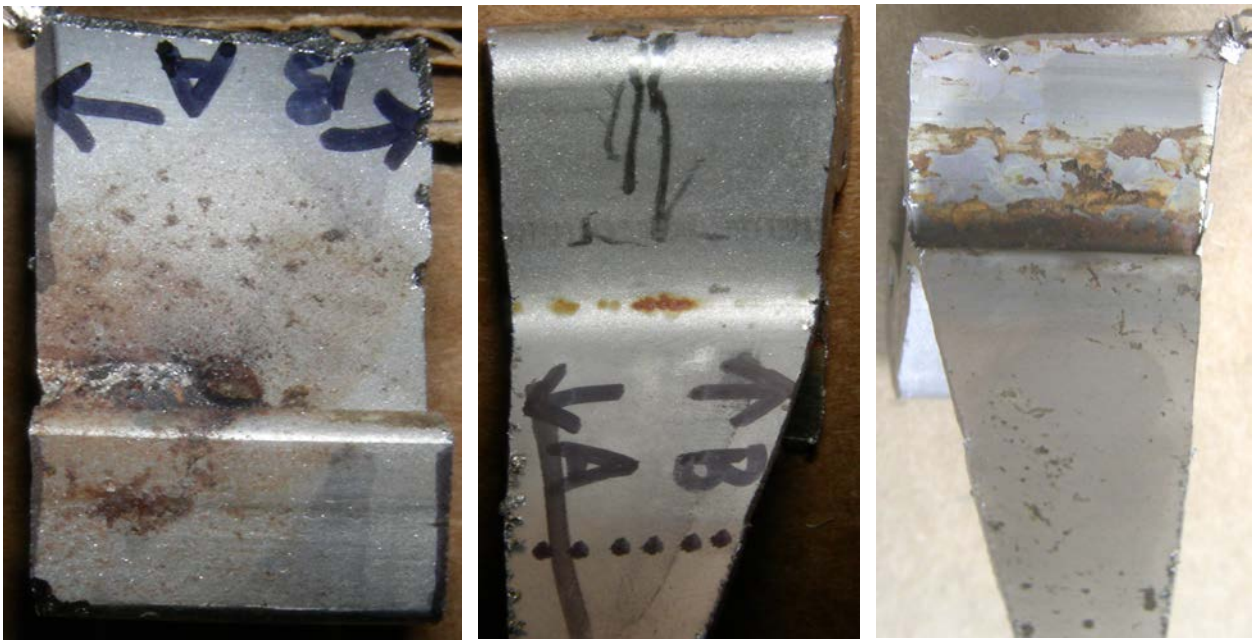

(a) Exterior side (b) Exterior bottom (c) Interior

Figure 25. Section removed from drum containing corrosion shown in Figure 21 (c).

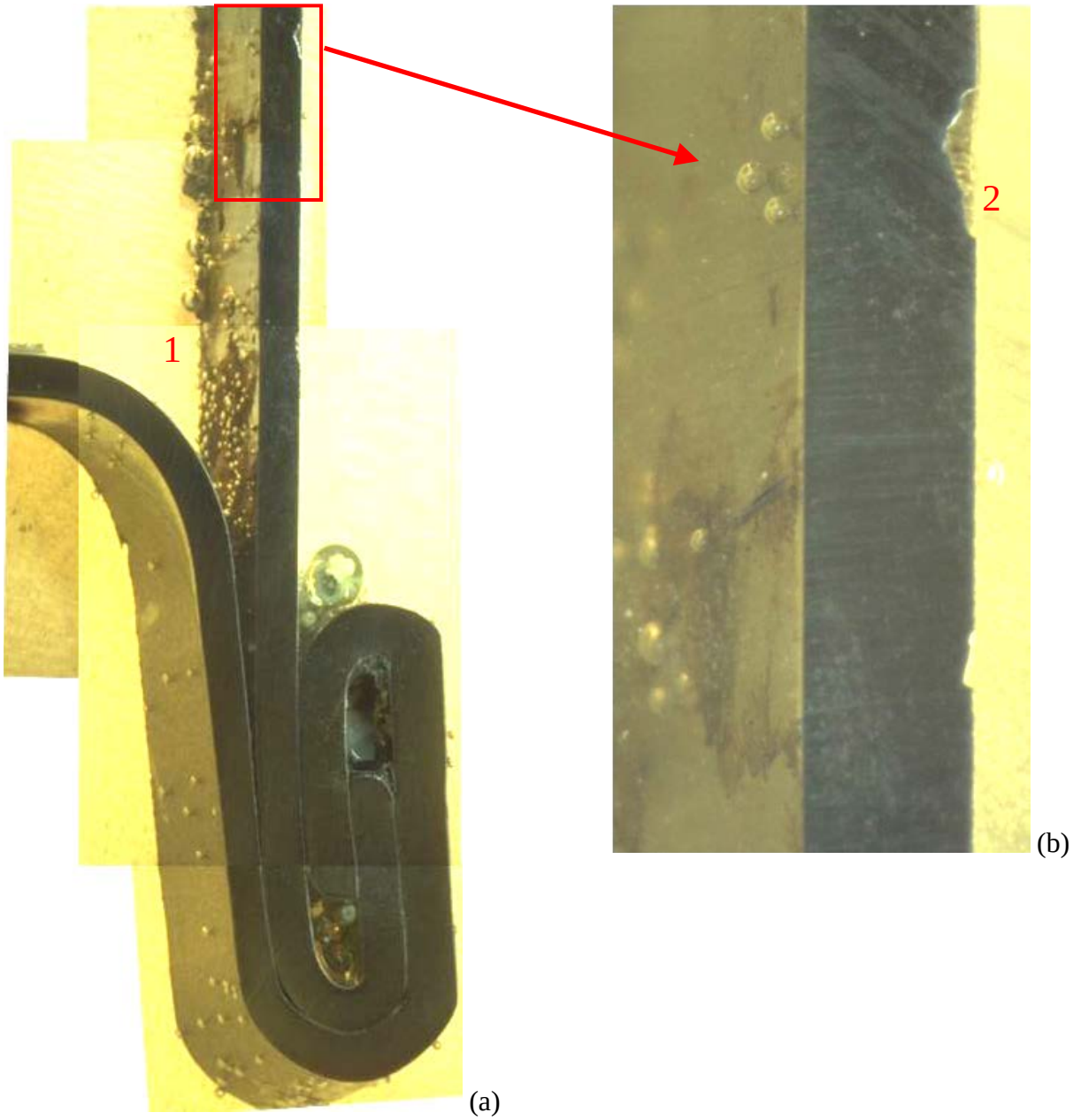

Figure 26. Cross section through the "B" half of the drum metallographic sample. Corrosion / scale on the drum interior surface is noted (1). Minor corrosion on the drum exterior sidewall (2) is shown in (b). Photos taken by 723-A Met Lab.

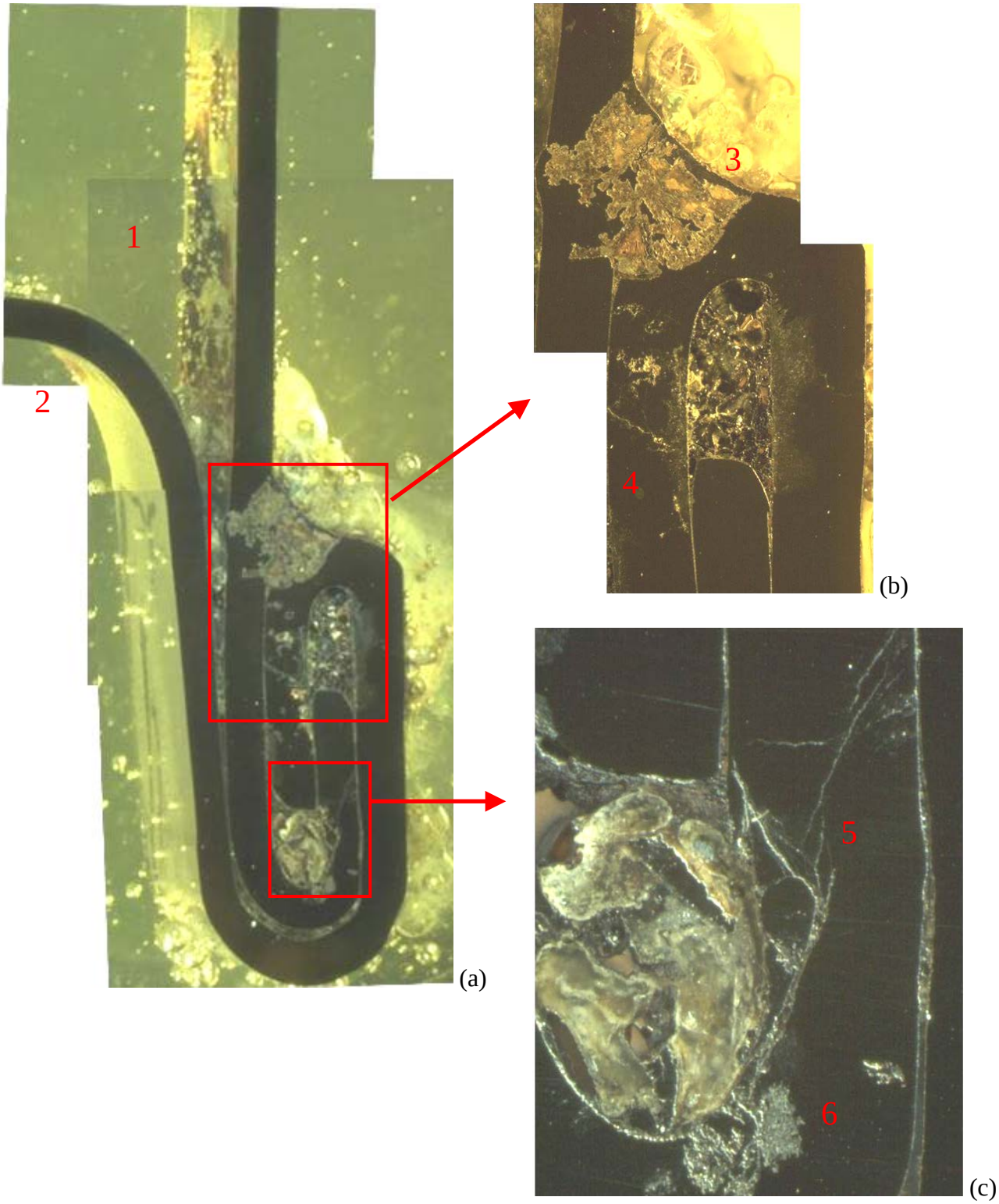

Figure 27. Cross section through the "A" half of the drum metallographic sample (a). Corrosion / scale on the drum interior (1) and exterior bottom (2) surfaces is noted. General/pitting corrosion (3, 6) and cracking (4, 5) are highlighted in (b) and (c), with penetration of the full wall thickness in some cases. Photos taken by 723-A Met Lab.

Attachment 1 9975-06100 Field Surveillance Results, with Comparison to Destructive Examination Results

Section I

Drum Exterior Examination

Item	Field Surveillance Result	Destructive Exam. Result
Drum vent plugs are specified and are in place as required	SAT	SAT
Drum surface is not dented beyond 0.25 inch	SAT	SAT
Drum Dents adjacent to the air shield are not deeper than 0.125 inch	SAT	SAT
Drum surface is free from corrosion, swelling/bulging and other physical damage	SAT	UNSAT

Comment – Corrosion was noted along bottom edge of drum in several spots, and on the bottom surface.

Section II

Humidity Measurements

Humidity at top of the drum	95.3 %RH	66.3 %RH on 8/20/15

Section III

Temperature Measurements

[These data not repeated in this report.]

Section IV

Celotex® Inspection

Upper Celotex® Assembly Weight: 26.3 lb (field surv.) 11.906 kg / 26.25 lb (destructive exam)

Visual:

Item	Field Surveillance Result	Destructive Exam. Result
Inspect all exposed Celotex® surfaces for significant damage and ensure layers are well bonded	SAT	SAT
Upper Celotex® came out smoothly, without interference	SAT	SAT
All visible Celotex® surfaces are free from staining and variation in coloration	UNSAT	UNSAT
Celotex® is free from significant swelling (e.g. gap exists against drum), shrinkage and other significant physical damage	UNSAT	SAT
Lead shield is free from significant deformation and physical damage and shows no sign of flaking, blistering or spalling	SAT	SAT
Lead shield Go/No Go gauge went smoothly into the lead shield and reached all the way to the bottom of the lead shield	SAT	NA

Comments: From field surveillance, “Evidence of water stains on upper celotex. Moldy smell evident w/ mold located on ¼ of upper celotex outer circumference.” From DE: “Upper fiberboard assembly – dark stains in some places (smeared glue?). Water stains on top of air shield, some running down side. Lower fiberboard assembly – mold on bottom ~2” of side, and some spots elsewhere on side. Dark stains on bottom (saturated) may mask possible mold on that surface. Bottom 1-2 layers has splitting / separation from drying & handling that was not present when opened before. One region on bottom has cracking due to drying.”

Attachment 1 9975-06100 Field Surveillance Results, with Comparison to Destructive Examination Results

Celotex® Dimensions (all results reported in inches)

Dimensions		0°	90°	180°	270°	Field Surveillance Average	Destructive Exam. Average
1	Upper Assembly OD	17.604	17.637			17.621	17.640
2	Upper Assembly lower step OD	14.728	14.672			14.700	14.685*
3	Upper Assembly ID	8.547	8.520			8.534	8.581
4	Upper Assembly inside height	4.936	4.943	4.933	4.975	4.947	4.983
5	Lower Assembly step height	1.959	1.999	2.056	2.045	2.015	2.020
6	Lower Assembly height from lower step to top of lead shield	4.509	4.521	4.543	4.518	4.523	NA

* calculated value

Dimension	Result	Criteria	Field Surveillance Result	Destructive Exam. Result
Dimension #4 average – Dimension #6 average	0.424	>0.425”	UNSAT	
Dimension #6 average	4.523	$\leq$ 4.65 ”	SAT	NA
Dimension #1 average – Dimension #3 average	9.087	$\geq$ 8 $^{3/16}$ ”	SAT	SAT

Section V

O-Ring Inspection

Test	SAT/UNSAT
O-ring seal test performed on SCV	SAT
SCV O-rings were removed intact	SAT
SCV O-rings have no excess accumulation of grease	SAT
O-ring seal test performed on PCV	SAT
PCV O-rings were removed intact	SAT
PCV O-rings have no excess accumulation of grease	SAT

Comments: n/a

Attachment 1 9975-06100 Field Surveillance Results, with Comparison to Destructive Examination Results

(all dimensional results reported in inches)

Action	0°	90°	180°	270°	Time	Destructive Exam. Average Result
Loosen SCV lid					1353	NA
Outer SCV O-Ring						
Measure OD (while on plug)	6.281	6.294			1401	NA
Measure radial thickness	0.1285	0.1240	0.1270	0.1335	1406	0.1382
Measure vertical thickness	0.1270				1405	0.1318
Inner SCV O-Ring						
Measure OD (while on plug)	6.173	6.169			1402	NA
Measure radial thickness	0.1240	0.1245	0.1240	0.1240	1404	0.1382
Measure vertical thickness	0.1325				1402	0.1323
Loosen PCV lid					1405	NA
Outer PCV O-Ring						
Measure OD (while on plug)	5.241	5.240			1411	NA
Measure radial thickness	0.1330	0.1260	0.1260	0.1310	1415	0.1358
Measure vertical thickness	0.1305				1414	0.1342
Inner PCV O-Ring						
Measure OD (while on plug)	5.118	5.112			1412	NA
Measure radial thickness	0.1350	0.1380	0.1385	0.1250	1414	0.1352
Measure vertical thickness	0.1280				1413	0.1358

Attachment 1 9975-06100 Field Surveillance Results, with Comparison to Destructive Examination Results

SRNL Receipt Examination of O-Rings

VISUAL EXAMINATION

PCV	PCV Outer	PCV Inner
Grease present	yes	no
Color (normal or explain)	Normal	Normal
Cross-sectional shape	round	round
Nicks, Scratches, Cracks	none	none
Other Damage (Note extent/size)	none	none
Picture (Note if taken)		

SCV	SCV Outer	SCV Inner
Grease present	yes	no
Color (normal or explain)	Normal	Normal
Cross-sectional shape	round, small step along mold line	round
Nicks, Scratches, Cracks	none	none
Other Damage (Note extent/size)	none	none
Picture (Note if taken)		

THICKNESS (all results reported in inches)

PCV	PCV Outer		PCV Inner	
	Axial	Radial	Axial	Radial
Thickness 1 (in)	0.1360	0.1360	0.1375	0.1340
Thickness 2 (in)	0.1370	0.1335	0.1350	0.1325
Thickness 3 (in)	0.1320	0.1325	0.1370	0.1315
Thickness 4 (in)	0.1350	0.1345	0.1335	0.1380
Field Surv. Average	**0.1350**	**0.1341**	**0.1358**	**0.1340**
Destructive Exam Average	**0.1342**	**0.1358**		

SCV	SCV Outer		SCV Inner	
	Axial	Radial	Axial	Radial
Thickness 1 (in)	0.1340	0.1360	0.1285	0.1400
Thickness 2 (in)	0.1325	0.1370	0.1345	0.1400
Thickness 3 (in)	0.1300	0.1355	0.1285	0.1360
Thickness 4 (in)	0.1305	0.1400	0.1310	0.1385
Field Surv. Average	**0.1318**	**0.1371**	**0.1306**	**0.1386**
Destructive Exam Average	**0.1318**	**0.1382**		

Attachment 1 9975-06100 Field Surveillance Results, with Comparison to Destructive Examination Results

SRNL Receipt Examination of O-Rings (Continued)

HARDNESS

	PCV O-Rings		SCV O-Rings	
	Outer	Inner	Outer	Inner
Hardness 1, M-Scale	71.0	68.5	69.0	72.0
Hardness 2, M-Scale	73.0	71.0	72.5	69.0
Hardness 3, M-Scale	71.0	74.0	73.0	75.0
Hardness 4, M-Scale	72.0	72.0	72.5	73.0
Hardness 5, M-Scale	71.0	72.0	71.0	72.0
Average	**71.6**	**71.9**	**71.3**	**72.2**

CONTINUATION:
NA

CC: R. J. Bayer, 705-K
J. S. Bellamy, 730-A
G. T. Chandler, 773-A
W. L. Daugherty, 773-A
K. A. Dunn, 773-41A
B. A. Eberhard, 105-K
B. L. Garcia-Diaz, 999-2W
L. F. Gelder, 999-W
T. W. Griffin, 705-K
T. J. Grim, 105-K
E. R. Hackney, 705-K
E. V. Henderson, 705-K
J. M. Jordan, 705-K
B. B. Kiflu, 705-K
D. R. Leduc, 730-A
J. W. McEvoy, 707-C
T. E. Skidmore, 730-A
D. E. Welliver, 705-K
K. E. Zeigler, 773-41A
Document Control